Tunable magnetization relaxation of $Fe_2Cr_{1-x}Co_xSi$ half-metallic Heusler alloys by band structure engineering

Shikun He,[1,2] Yifan Liu,[3] Yuhong Zheng,[3] Qing Qin,[4] Zhenchao Wen,[5] Qingyun Wu,[6] Yi Yang,[2] Yupu Wang,[3] YuanPing Feng,[6] Kie Leong Teo,[3,*] and Christos Panagopoulos[1,†]

[1]*Division of Physics and Applied Physics, School of Physical and Mathematical Sciences, Nanyang Technological University, Singapore 637371*

[2]*Data Storage Institute, Agency for Science, Technology and Research (A*STAR), 2 Fusionopolis Way 08-01 Innovis, Singapore 138634*

[3]*Department of Electrical and Computer Engineering, National University of Singapore, Singapore 117582*

[4]*Department of Materials Science and Engineering, National University of Singapore, Singapore 117574*

[5]*Center for Spintronics Research Network (CSRN), Tohoku University, Sendai 980-8577, Japan*

[6]*Department of Physics, National University of Singapore, Singapore 117542*

(Received 24 June 2017; revised manuscript received 13 August 2017; published 1 November 2017)

We report a systematic investigation on the magnetization relaxation properties of iron-based half-metallic Heusler alloy $Fe_2Cr_{1-x}Co_xSi$ (FCCS) thin films using broadband angular-resolved ferromagnetic resonance. Band structure engineering through Co doping (x) demonstrated by first-principles calculations is shown to tune the intrinsic magnetic damping over an order of magnitude, namely 1×10^{-2}–8×10^{-4}. Notably, the intrinsic damping constants for samples with high Co concentration are among the lowest reported for Heusler alloys and even comparable to magnetic insulator yttrium iron garnet. Furthermore, a significant reduction of both isotropic and anisotropic contributions of extrinsic damping of the FCCS alloys was found in the FCCS films with $x = 0.5$–0.75, which is of particular importance for applications. These results demonstrate a practical recipe to tailor functional magnetization for Heusler alloy-based spintronics at room temperature.

DOI: 10.1103/PhysRevMaterials.1.064401

I. INTRODUCTION

Control of magnetization and its dynamics in nanomagnets by injecting an electrical current is increasingly important [1,2]. Operations based on spin transfer torque (STT) are energy efficient with superior scalability for high density device applications compared to conventional methods employing magnetic fields [3–6]. A promising application of STT is nonvolatile magnetic random access memory (MRAM) [7,8]. The key parameter here is magnetic damping; it determines the critical switching current and speed of magnetization reversal [2,9]. Hence, a magnetic material with tunable low damping is needed. Magnetic relaxation is primarily due to spin-orbit coupling (SOC), however, materials and device guidance from theoretical calculations is hindered by the complicity of inter- and intraband scattering, defects, disorder, interface effects, and geometrical confinement [10,11]. A practical criterion for engineering magnetic damping is $\alpha \propto \xi^2 D(E_F)$ [12,13], where ξ is the SOC parameter and $D(E_F)$ is the density of states (DOS) at the Fermi level. Although Fe, Co, and Ni render the window for tunable SOC in $3d$-based materials formidably narrow, there have been encouraging developments through the correlation between damping and electronic structure, as demonstrated in FeV and CoFe binary alloys [14,15]. Still, reducing and tuning magnetic damping in metallic materials can be difficult due to magnon scattering by high density conduction electrons [10]. Notably, the lowest reported damping for CoFeB, the material employed by industry for MRAM development, is approximately 0.004 [16,17].

Half-metallic Heusler alloy is a semiconductor for one spin projection and a metal for the other [18], hence the band structure is expected to result in high spin polarization and low damping [19–23]. Both properties are favorable for STT [9]. However, except for a few Co-based Heusler alloys, the damping constant is larger than for Fe films (0.002), probably due to band broadening by structural defects, chemical disorder, and magnon excitation [13,24–28]. Furthermore, Heusler alloys usually exhibit large anisotropy in the ferromagnetic resonance (FMR) linewidth [26,29], which may lead to large variation in performance among devices. Therefore, tuning and reducing intrinsic damping and a minimum extrinsic magnetic relaxation are required for reliable operations. Fe-based Heusler alloys are expected to possess half-metallic band structure [30]. Also, these materials hold great promise for high interfacial perpendicular anisotropy [31], an indispensable property for next generation STT-MRAM, at a Fe-MgO interface [32,33]. However, a comprehensive magnetization relaxation study is still lacking for Fe-based Heusler alloys.

Here we tune the band structure of $Fe_2Cr_{1-x}Co_xSi$ (FCCS) by Co doping (x). Dynamic and static properties were investigated using angle-resolved broadband FMR. We show ordered states ($B2$ and $L2_1$) exhibit considerably lower damping compared to disordered states ($A2$). Crucially, Co doping allows control of the intrinsic damping constant by an order of magnitude (1×10^{-2}–8×10^{-4}). Furthermore, both isotropic and anisotropic extrinsic contributions to the in-plane magnetization relaxation of quaternary FCCS can be significantly reduced for x between 0.5 and 0.75.

II. EXPERIMENT

The samples were prepared in an ultrahigh vacuum magnetron sputtering system with base pressure 10^{-7} Pa. Prior to deposition, the MgO (100) substrate was heated at 600 °C for 1 h. Subsequently, a 40 nm Cr buffer layer was deposited

*eleteokl@nus.edu.sg
†christos@ntu.edu.sg

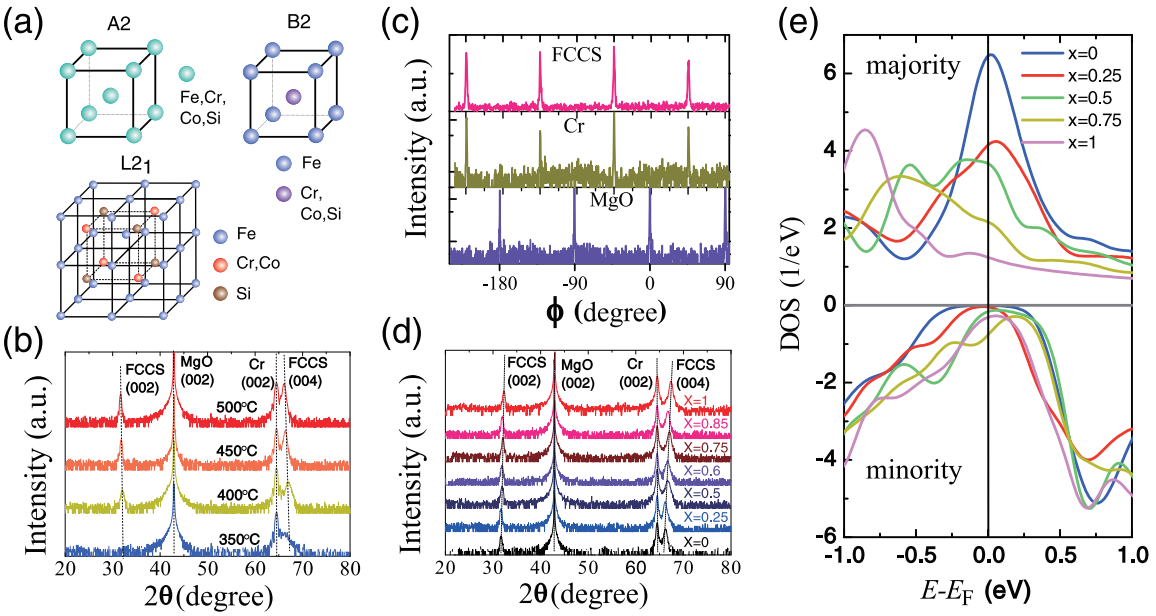

FIG. 1. Structures of the films with stacks of MgO(001)-substrate (30 nm)/Cr (40 nm)/$Fe_2Cr_{1-x}Co_xSi$ (30 nm)/Ru (3 nm). (a) Schematics of the disordered $A2$, partially ordered $B2$, and ordered $L2_1$ structures. (b) XRD θ-2θ scans for $Fe_2Cr_{0.5}Co_{0.5}Si$ thin films with various *in situ* annealing temperatures. (c) ϕ scans of FCCS, Cr, and MgO of MgO(001)-substrate/Cr(40 nm)/Fe2Cr0.5Co0.5Si(30 nm)/Ru(3 nm) for the (111) plane. The *in situ* annealing temperature is 450 °C. (d) XRD θ-2θ scans for $Fe_2Cr_{1-x}Co_xSi$ with various Co concentrations. The films were *in situ* annealed at 450 °C. (e) Density of states (DOS) of FCCS alloys determined by first-principle calculations.

followed by 1 h *in situ* annealing at 700 °C. The quaternary Heusler alloy FCCS (30 nm) layer with variable Co doping was deposited by co-sputtering Fe_2CrSi and Fe_2CoSi. The deposition speed of an individual target, hence the nominal value of x, was tuned by adjusting the sputtering power. Total deposition rate was approximately 0.3 Å/s for smooth growth. An *in situ* annealing procedure was performed at T_{ia} for 30 min to develop ordered $B2$ or $L2_1$ structures. A series of T_{ia} (350–500 °C) was used for $x = 0.5$, whereas T_{ia} was fixed at 450 °C for all other samples. Finally, the FCCS layer was capped by Ru (3 nm) to avoid oxidation.

Our homebuilt angular-resolved FMR system equipped with an Agilent E8361C vector network analyzer (VNA) can measure with frequency up to 40 GHz. We use a grounded coplanar waveguide with a nominal impedance of 50 Ω and a center conductor of width 100 μm [16]. A customized sample holder is attached to a motorized stage for out-of-plane field rotation. In addition, an in-plane sample manipulator is used to rotate and mount the sample face down on the waveguide automatically. The accuracy of in-plane and out-of-plane field orientations is better than 0.1 deg. Using angle-resolved broadband FMR, we determine the intrinsic damping by measuring with magnetization perpendicular to the film plane, whereas the anisotropy in magnetization relaxation was investigated by varying the magnetization orientation within the film plane.

III. RESULTS AND DISCUSSION

A. Structure and chemical ordering

As shown in Fig. 1(a), there are three structures in a FCCS Heusler alloy film according to their atomic ordering: fully ordered full-Heulse $L2_1$ structure, partially disordered $B2$, and fully disordered $A2$ structures.

FCCS(002) peaks of XRD θ-2θ scans of $Fe_2Cr_{0.5}Co_{0.5}Si$ films [Fig. 1(b)] indicate that ordering of the FCCS film evolves from $A2$ to $B2$ or $L2_1$ for $T_{ia} = 400$ °C. The Cr and FCCS layers exhibit epitaxial growth at 45° with respect to MgO substrate (XRD phi-scan in Fig. 1(c) and see the Supplemental Material Fig. S4 for transmission electron microscopy results [34]). The degree of $B2$ ordering (S_{B2}) and $L2_1$ ordering (S_{L2_1}) was calculated using the Webster model [35]. Best crystalline structure with $S_{B2} = 0.95$ and $S_{L2_1} = 0.87$ was obtained for $T_{ia} = 450$ (see the Supplemental Material Fig. S1(a) for T_{ia} dependence of ordering [34]). Correspondingly, the saturation magnetization M_s increases with T_{ia} reaching maximum at $T_{ia} = 450$ °C (see the Supplemental Material Fig. S2 for T_{ia} dependence of M_s [34]). Furthermore, $B2$ and $L2_1$ phases were obtained for all Co concentrations with $T_{ia} = 450$ °C as inferred from 1(d). All samples exhibited a high degree of $B2$ ordering ($S_{B2} > 0.74$) and moderate $L2_1$ ordering (see the Supplemental Material Fig. S1(b) for Co concentration dependence of ordering [34]). The $B2$ phase characterized by Y-Z atomic disorder in the Fe-based X_2YZ full-Heusler alloy is also favorable for device applications since it smears the DOS spectral shapes, does not degrade half-metallicity significantly, and has little influence on damping [30,36,37]. Our first-principles calculations (see the Supplemental Material Fig. S3 for calculation methods [34]) have shown that the band structures of $L2_1$ FCCS were successfully tuned by Co concentration. As can be clearly seen from Fig. 1(e), Fe_2CrSi and $Fe_2Cr_{0.75}Co_{0.25}Si$ exhibit half-metallicity, whereas for $x \geqslant 0.5$, the minority band DOS at the Fermi level is nonzero and increases with x. On the other hand, the total DOS at Fermi level dominated by the majority band decreases monotonically with x.

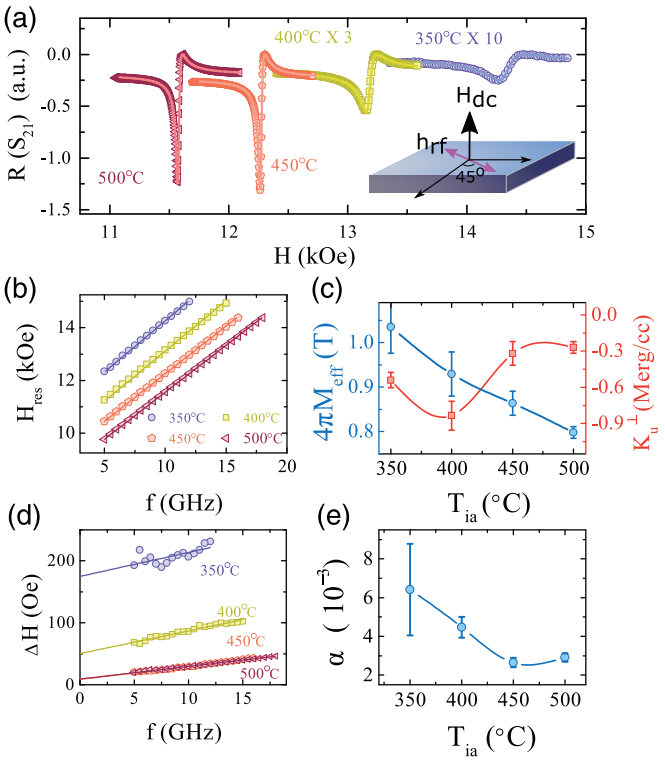

FIG. 2. Room temperature out-of-plane FMR results of $Fe_2Cr_{0.5}Co_{0.5}Si$ for different *in situ* annealing temperature T_{ia}. (a) Field dependence of the amplitude of FMR spectra for $f =$ 10 GHz. The inset is an illustration of the measurement configuration. (b) Frequency dependence of FMR resonance field. (c) Effective magnetization and perpendicular anisotropy versus T_{ia}. (d) Frequency dependence of FMR linewidth. (e) Damping as a function of T_{ia}.

B. Dynamic properties of $Fe_2Cr_{0.5}Co_{0.5}Si$

Room temperature out-of-plane FMR spectra were taken with $\varphi_H = \pi/4$. Figure 2(a) shows FMR data for $Fe_2Cr_{0.5}Co_{0.5}Si$ at different T_{ia}. Stronger signals and narrower peaks are observed for $T_{ia} > 400\,^{\circ}$C. The narrowest spectrum is for $T_{ia} = 450\,^{\circ}$C, in correspondence with the structure and magnetization measurements [38]. The resonance field H_{Res} and full width at half maximum (FWHM) ΔH were extracted by modified Lorentz fit (see the Supplemental Material Fig. S2 for the fitting method [34]). The frequency dependencies of H_{Res} are shown in Fig. 2(b). The Kittel equation describing the resonance condition for out-of-plane configuration is given by

$$2\pi f = \gamma(H - 4\pi M_{\text{eff}}), \tag{1}$$

indicating the linear relation between resonance frequency and field. Here $\gamma = ge/2m_e$ is the gyromagnetic ratio determined by the Lande g factor, electron charge e, and mass m_e. $4\pi M_{\text{eff}}$ is the effective saturation magnetization $4\pi M_{\text{eff}} = 4\pi M_s - 2K_u^{\perp}/M_s = 4\pi M_s - H_k$, $K_u^{\perp}$ is the perpendicular anisotropy, and H_k is the anisotropy field. The data are well fitted by straight lines. Using the slope, intercept of the fit, and M_s, which we measure using a vibrating sample magnetometer (see the Supplemental Material Fig. S2 [34]), we determined the value of g, $4\pi M_{\text{eff}}$, and $K_u^{\perp}$. As seen from Fig. 2(c), the films possess a negative $K_u^{\perp}$ (easy axis in the film plane). We find the corresponding H_k to be of the order of kOe, considerably larger than the in-plane anisotropy field, which we discuss later. We believe $K_u^{\perp}$ originates from interfacial stress and varies with T_{ia} due to the annealing temperature dependence of ordering and lattice constant [24]. Figure 2(d) indicates the FMR linewidth increases linearly with frequency for all samples. This allows the determination of damping constant α through

$$\Delta H_{\text{OP}} = \frac{4\pi}{\gamma}\alpha f + \Delta H_0. \tag{2}$$

Here α is the coefficient of the viscous phenomenological dissipation term after Gilbert [39]. ΔH_0 is the inhomogeneous broadening due to the dispersion of magnetic properties. The damping constant for FCCS film with optimal $L2_1$ and $B2$ phase is $(2.6 \pm 0.3) \times 10^{-3}$, i.e., 40 percent the value of the $A2$ phase [$(6.5 \pm 0.2) \times 10^{-3}$, Fig. 2(e)]. The results indicate the ordered half-metallic phase has lower damping, suggesting atomic chemical disorder enhances damping [10]. Clearly, annealing at $T_{ia} \geqslant 400\,^{\circ}$C improves sample uniformity as inferred from the T_{ia} dependence of ΔH_0.

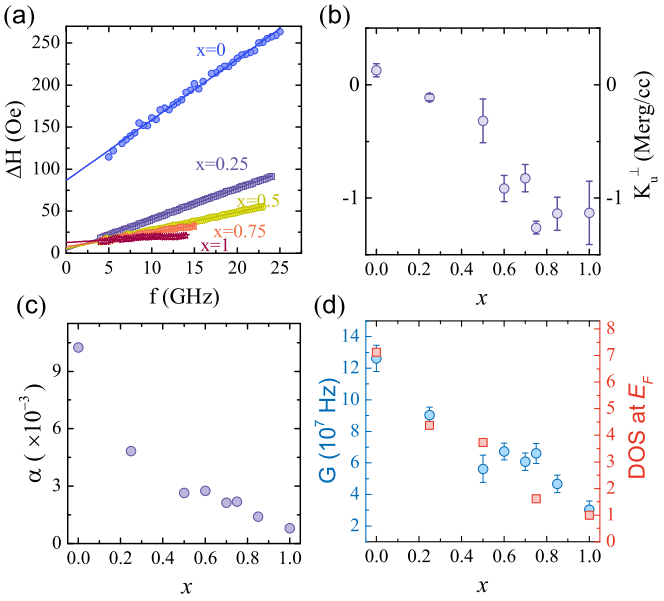

FIG. 3. Co concentration dependence of FMR results in $Fe_2Cr_{1-x}Co_xSi$. (a) FMR linewidth versus frequency for various values of x. The solid lines are linear fits to the data. (b) Perpendicular uniaxial magnetic anisotropy versus x. (c) Damping constant α versus x. (d) Relaxation frequency G and total density of states at the Fermi level versus x.

C. Co doping dependence of magnetization relaxation of $Fe_2Cr_{1-x}Co_xSi$

The out-of-plane FMR results with a magnetic field up to 2.1 T for a series of FCCS samples are shown in Fig. 3. All samples were annealed at $T_{ia} = 450\,^{\circ}$C. Again, we find linear frequency dependencies of the linewidth. The perpendicular anisotropy constant and damping values shown in Figs. 3(b) and 3(c) were determined using the same procedure described earlier. $K_u^{\perp}$ increases with x may be attributed to the Co doping dependence of tetragonal distortion [40], determined by the reciprocal space mapping (see the

Supplemental Material Fig. S3 for structural information [34]). Damping for Fe_2CrSi ($x = 0$) is the largest $(1 \pm 0.03) \times 10^{-2}$. For $x = 0.25$, damping decreases by approximately 50% to $(4.8 \pm 0.1) \times 10^{-3}$. Further increase of Co doping results in a nearly linear reduction in damping. Fe_2CoSi ($x = 1$) exhibits the lowest damping $(8 \pm 1) \times 10^{-4}$; this is considerably lower than $3d$ metals and remarkably close to the value for high quality $Y_3Fe_5O_{12}$ (YIG) films [41,42].

Relaxation frequency $G = \gamma M_s \alpha$ is directly related to the speed of relaxation and decreases by a factor of 4 with increasing x. The lowest relaxation frequency (30 MHz) observed in Fe_2CoSi [Fig. 3(d)] is comparable to that in FeV films [14]. The offset to smaller α and G for $x = 0.5$ is because T_{ia} was optimized at this particular value of x. Hence, damping can be reduced further by fine tuning growth conditions.

Magnetic damping depends on SOC and DOS $G \propto \xi^2 D(E_F)$ [43]. Low ξ in Heusler compounds because of quenching of orbital moments [13] and suppression of interband scattering [11] due to relatively high spin-polarization band structure may account for the overall low damping. On the other hand, the x dependence of relaxation frequency is due to band structure engineering as shown in Fig. 1(d), indicated by the simultaneous decrease of relaxation frequency and total DOS at the Fermi level with x. A small misalignment may be due to band broadening by defects and chemical disorder.

Similarly, according to Du *et al.*, the Fermi level of FCCS ingots moves from the bottom of the conduction band to the top of the valence band with increasing x for the minority band [44]. The observed band structure tuning effect of Fe-based Heusler alloys also agrees with earlier investigations on Co-based Heusler compounds [28].

D. Anisotropic magnetization relaxation of $Fe_2Cr_{1-x}Co_xSi$

Using out-of-plane FMR measurements, we determined the intrinsic damping by purposely suppressing the extrinsic contributions causing nonlinear frequency dependence [16,17,45]. In practical applications, the relaxation mechanism for magnetization in the film plane is of primary importance. Hence, we investigated the FCCS samples using in-plane magnetic field. The azimuthal angle (φ_H) dependence of resonance field shows fourfold symmetry [Fig. 4(a)], indicative of a dominant in-plane cubic magnetocrystalline anisotropy. Uniaxial anisotropy, on the other hand, is negligible. The in-plane magnetic easy axis is along [110] of the substrate as the minimum of resonance field occurs at $\varphi_H = \pi/4$ and $\varphi_H = 3\pi/4$, along which the lattice constant of FCCS matches MgO. We fit the data using the following equation derived from Smit-Beljers formula [46,47]:

$$2\pi f = \gamma \sqrt{UV}, \tag{3}$$

where $U = H\cos(\varphi_M - \varphi_H) + 4\pi M_{\text{eff}} + K^{4\parallel}/2M_s[3 + \cos 4(\varphi_M - \pi/4)]$ and $V = H\cos(\varphi_M - \varphi_H) + 2K^{4\parallel}/M_s \cos 4(\varphi_M - \pi/4)$, φ_M and φ_H are the orientation of magnetization and external field with respect to [100] direction of MgO. As shown in Fig. 4(b), the in-plane fourfold anisotropy energy increases with Co composition. The corresponding anisotropy field $H^{4\parallel} = 2K^{4\parallel}/M_s$ observed in Fe_2CoSi is approximately 190 Oe. The φ_H dependence of FMR linewidth changes

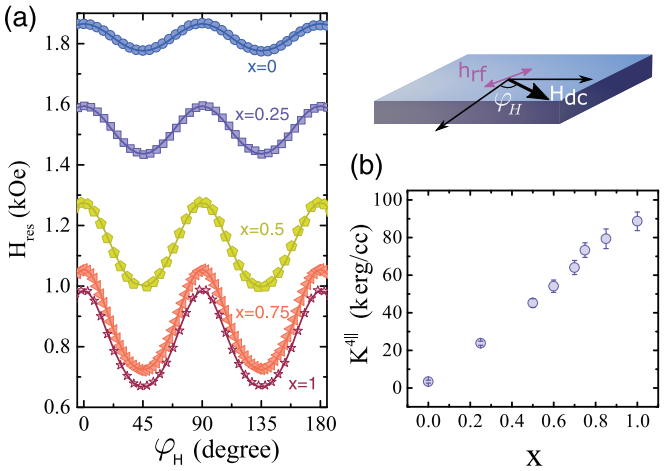

FIG. 4. Room temperature in-plane FMR resonance fields and anisotropic energy. (a) In-plane FMR resonance field at $f = 10$ GHz as a function of field direction for $Fe_2Cr_{1-x}Co_xSi$ samples with different Co concentration. Solid lines are calculated using Eq. (3). (b) Co concentration dependence of in-plane fourfold anisotropy energy. The schematic on the top right shows the coordinates used in the measurements and the orientations of dc and rf fields.

dramatically with x, Fig. 5(d). For Fe_2CrSi, we observe a nearly fourfold symmetry with minimum at $\varphi_H = 0$ ([100]), conversely, smallest linewidth occurs around $\varphi_H = \pi/4$, characteristic of Fe_2CoSi. Notably, the linewidth anisotropy is much lower for FCCS films than for Fe_2CrSi and Fe_2CoSi.

The anisotropy in the linewidth may be attributed to angle dependent damping [48] or an extrinsic origin [24]. Recent calculations show that anisotropy in intrinsic damping is small at room temperature [49,50]. Therefore, extrinsic linewidth broadening mechanisms, such as angle dependent inhomogeneous contribution and spin wave scattering should be considered. In general, the measured linewidth is the sum of intrinsic and extrinsic contributions [48,51,52]:

$$\Delta H = \Delta H_{\text{int}} + \left|\frac{\partial H_{\text{Res}}}{\partial 4\pi M_{\text{eff}}}\right| \Delta 4\pi M_{\text{eff}} + \left|\frac{\partial H_{\text{Res}}}{\partial H_K}\right| \Delta H_K + \Delta H_{\text{TMS}}. \tag{4}$$

The first term on the right-hand side is the intrinsic linewidth [Fig. 5(a)]. For noncollinear magnetization and external field ($\varphi_H \neq \varphi_M$), the magnetization direction changes during field sweep, giving additional broadening to the intrinsic linewidth. In the present case of a relatively small in-plane anisotropy, the effect is calculated numerically to the first order using the resonance field together with the equilibrium condition for magnetization [48,51,53]: $\Delta H_{\text{int}} = \frac{1}{|2\pi \partial f/\partial H|}\frac{\alpha}{\gamma}(U + V) \approx \frac{4\pi\alpha}{\gamma \cos(\varphi_M - \varphi_H)} f$. The second and third terms are due to dispersion of the effective magnetization and anisotropy field, respectively [Fig. 5(b)]. The partial derivatives are evaluated numerically at the resonance condition. The last term accounts for two magnon scattering (TMS) [54,55] activated by defects such as dislocations (see the Supplemental Material Fig. S4 for TEM results [34]), representing relaxation of the uniform mode to spin wave modes of nonzero wave vector [Fig. 5(c)]. We fit the data in Fig. 5(d) by adopting a phenomenological form of TMS linewidth $\Delta H_{\text{TMS}} = \Gamma_1 + \Gamma_2 \cos^2(2\varphi_M - \phi_{\max})$

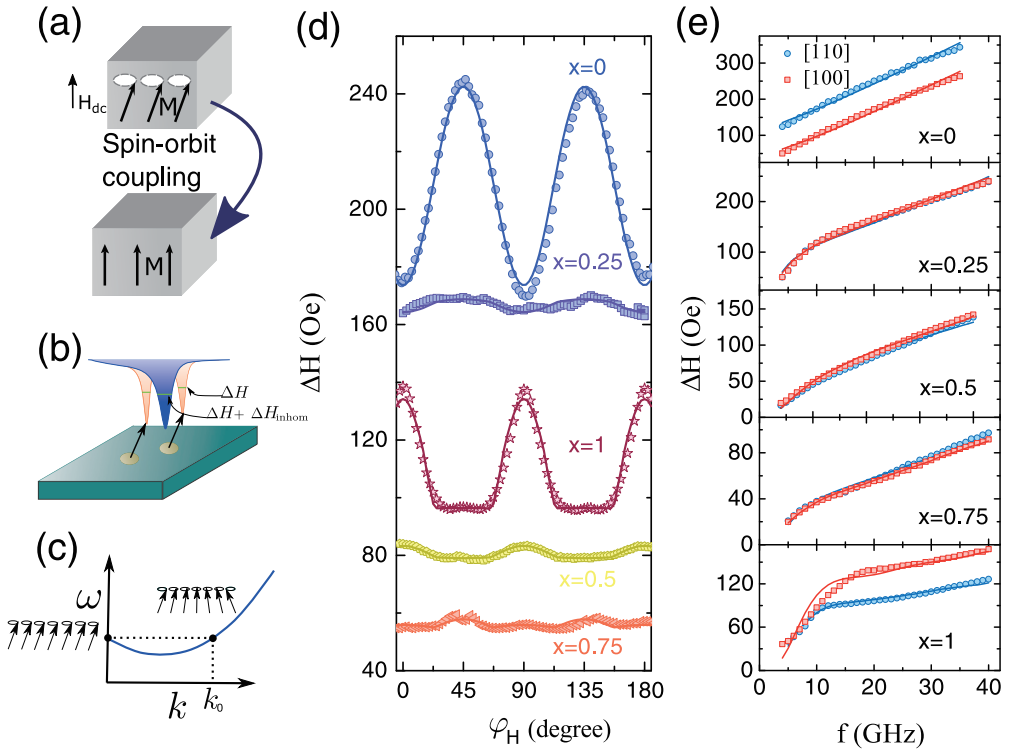

FIG. 5. In-plane angular and frequency dependence of FMR linewidth of $Fe_2Cr_{1-x}Co_xSi$. (a)–(c) Illustrations of magnetization relaxation due to spin-orbit coupling (a), inhomogeneity (b), and scattering by magnon excitation (c). (a) Intrinsic damping is caused by spin-orbit coupling. (b) Sample inhomogeneity broadens the FMR linewidth as the spectrum is a superposition of local resonance. (c) The uniform precession mode of FMR can be scattered to degenerate spin-wave mode. (d) In-plane FMR linewidth for $f = 20$ GHz as a function of field direction for FCCS samples with different Co concentration; solid lines are fits to the data using Eq. (4). (e) Frequency dependence of FMR linewidth for magnetization along [110] and [100] directions. The solid lines are fits to the data using Eqs. (4) and (5).

[24,26]. Here Γ_1 and Γ_2 are the isotropic and anisotropic TMS amplitude, respectively. The anisotropic term correlates to defects of preferential orientation [56]. $\phi_{\max}$ is the orientation along which the 2D Fourier transformation of defects potential shows a maximum. We fit the data for all Co dopings. The extracted parameters are shown in Figs. 6(a) and 6(c). Although the anisotropic extrinsic damping of FCCS appears universal in Hesuler alloys [29], when compared to Fe_2CrSi and Fe_2CoSi, it is considerably lower and almost vanishes for $0.5 \leqslant x \leqslant 0.75$.

To study further the extrinsic relaxation and its anisotropy, we measured the frequency dependence of FMR linewidth for magnetization along the in-plane easy MgO[110] and hard MgO[100] axes. Figure 5(e) depicts significant differences between the two magnetization orientations observed only for $x = 0$ and $x = 1$, in agreement with the angular dependence data. On the other hand, a nonlinearity as a signature of TMS was observed in all samples. We calculated the magnon wave vector (k_0) at which the spin wave energy degenerates with the uniform modes $\omega(k_0) = 2\pi f$ for a given propagation direction φ with respect to magnetization in the film plane [56,57]. The total contribution to TMS was then estimated using [58,59]

$$\Delta H_{\mathrm{TMS}} = \frac{2K}{\gamma^2}\frac{\partial f}{\partial H}\int \frac{k_0}{df/dk}d\varphi, \qquad (5)$$

where df/dk was evaluated at k_0 and $\partial f/\partial H$ calculated from the FMR resonance conditions. $K = 0.16h^2A_\xi$ is the only fitting parameter related to defects. The fits to the frequency dependence of linewidths are shown by solid lines. The fitting parameter K for both magnetization orientation and their difference $\Delta K = K_{[100]} - K_{[110]}$ are indicative of the strength of TMS and its anisotropy, respectively. The fitting results are plotted in Figs. 6(b) and 6(d). The Co doping dependence of $K_{[110]}$ agrees with the trend obtained earlier from the angular dependence of the linewidth.

The anisotropy in TMS (ΔK) is maximum for $x = 1$ and negligible for x around 0.7. Furthermore, we obtain a relatively small anisotropy of TMS for $x = 0$, as expected from the weak nonlinearity of the two curves shown in the top panel of Fig. 5(e). However, the results appear inconsistent with the phenomenological fit shown in Fig. 6(a). We attribute this to orientation dependent long range inhomogeneity in the sample, apparent also from the large zero frequency broadening (ΔH_0) in Fig. 3(a) for $x = 0$. Here the phenomenological fit cannot separate the angular dependence of inhomogeneous broadening from fourfold TMS, hence overestimating the TMS contribution for $x = 1$. Nevertheless, both the frequency dependence and angular dependence of the linewidths are in agreement, confirming that the isotropic and anisotropic extrinsic damping constants of FCCS are significantly reduced for $x = 0.5$–0.75. Therefore, in FCCS with $0.5 \leqslant x \leqslant 0.75$,

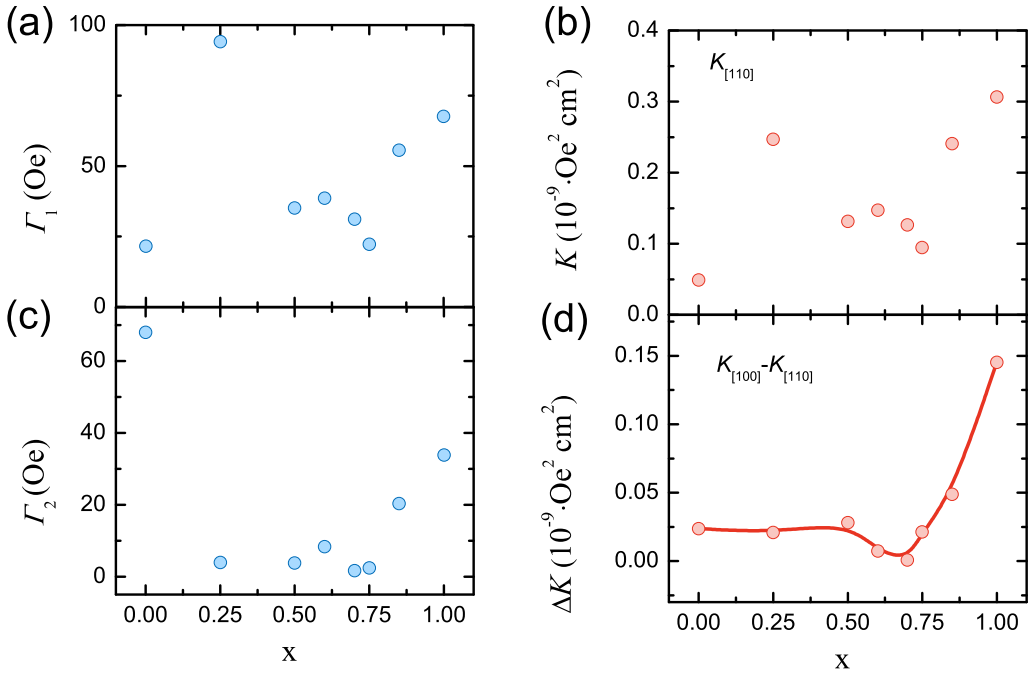

FIG. 6. Isotropic and anisotropic TMS contributions in $Fe_2Cr_{1-x}Co_xSi$. (a) and (c) Isotropic and anisotropic components of the TMS linewidth determined by the phenomenological method of angular dependent linewidth. (b) and (d) Co concentration dependence of K for magnetization along [110] and anisotropy of K.

low damping and nearly isotropic response are promising for practical applications.

In summary, we studied the structure order and composition dependence of magnetization relaxation in $Fe_2Cr_{1-x}Co_xSi$ Heusler alloy thin films. We show the ordered phase has a low intrinsic damping, tunable by Co doping. Notably, the anisotropic extrinsic relaxation of the quaternary alloys can be significantly reduced for FCCS films with $x = 0.5$–0.75. Furthermore, perpendicular and in-plane magnetic anisotropy show nearly linear dependence on Co doping. The present work demonstrates the tunable nature of both static and dynamic magnetic properties of Fe-based Heusler alloys. The engineered low damping constant in $Fe_2Cr_{1-x}Co_xSi$ thin films encourages the utilization of Heusler alloys in room temperature spintronics.

ACKNOWLEDGMENTS

The work was supported by the Ministry of Education (MOE), Academic Research Fund (AcRF) Tier 2 Grant (MOE2014-T2-1-050), the A*STAR Pharos Fund (1527400026), and the National Research Foundation (NRF-CRP12-2013-01), NRF-Investigatorship (NRF-NRFI2015-04). The authors acknowledge the Singapore Synchrotron Light Source (SSLS) for providing the facilities to perform x-ray experiments.

S.H. and Y.L. contributed equally to this work.

[1] L. Berger, Phys. Rev. B **54**, 9353 (1996).
[2] J. C. Slonczewski, J. Magn. Magn. Mater. **159**, L1 (1996).
[3] S. Ikeda, K. Miura, H. Yamamoto, K. Mizunuma, H. D. Gan, M. Endo, S. Kanai, J. Hayakawa, F. Matsukura, and H. Ohno, Nat. Mater. **9**, 721 (2010).
[4] K. Wang, J. Alzate, and P. K. Amiri, J. Phys. D **46**, 074003 (2013).
[5] D. Worledge, G. Hu, D. W. Abraham, J. Sun, P. Trouilloud, J. Nowak, S. Brown, M. Gaidis, E. O'sullivan, and R. Robertazzi, Appl. Phys. Lett. **98**, 022501 (2011).
[6] A. D. Kent and D. C. Worledge, Nat. Nanotech. **10**, 187 (2015).
[7] M. Gajek, J. Nowak, J. Sun, P. Trouilloud, E. O'sullivan, D. Abraham, M. Gaidis, G. Hu, S. Brown, Y. Zhu *et al.*, Appl. Phys. Lett. **100**, 132408 (2012).
[8] L. Thomas, G. Jan, J. Zhu, H. Liu, Y.-J. Lee, S. Le, R.-Y. Tong, K. Pi, Y.-J. Wang, D. Shen *et al.*, J. Appl. Phys. **115**, 172615 (2014).
[9] S. Mangin, D. Ravelosona, J. A. Katine, M. J. Carey, B. D. Terris, and E. E. Fullerton, Nat. Mater. **5**, 210 (2006).
[10] A. A. Starikov, P. J. Kelly, A. Brataas, Y. Tserkovnyak, and G. E. W. Bauer, Phys. Rev. Lett. **105**, 236601 (2010).
[11] K. Gilmore, Y. U. Idzerda, and M. D. Stiles, Phys. Rev. Lett. **99**, 027204 (2007).
[12] V. Kamberský, Czech. J. Phys. **34**, 1111 (1984).
[13] S. Trudel, O. Gaier, J. Hamrle, and B. Hillebrands, J. Phys. D **43**, 193001 (2010).
[14] C. Scheck, L. Cheng, I. Barsukov, Z. Frait, and W. E. Bailey, Phys. Rev. Lett. **98**, 117601 (2007).

[15] M. A. W. Schoen, D. Thonig, M. L. Schneider, T. J. Silva, H. T. Nembach, O. Eriksson, O. Karis, and J. M. Shaw, Nat. Phys. **12**, 839 (2016).

[16] S. He and C. Panagopoulos, Rev. Sci. Instrum. **87**, 043110 (2016).

[17] A. Okada, S. He, B. Gu, S. Kanai, A. Soumyanarayanan, S. Ter Lim, M. Tran, M. Mori, S. Maekawa, F. Matsukura *et al.*, Proc. Natl. Acad. Sci. USA **114**, 3815 (2017).

[18] M. Katsnelson, V. Y. Irkhin, L. Chioncel, A. Lichtenstein, and R. De Groot, Rev. Mod. Phys. **80**, 315 (2008).

[19] C. Liu, C. K. A. Mewes, M. Chshiev, T. Mewes, and W. H. Butler, Appl. Phys. Lett. **95**, 022509 (2009).

[20] M. Jourdan, J. Minár, J. Braun, A. Kronenberg, S. Chadov, B. Balke, A. Gloskovskii, M. Kolbe, H. Elmers, G. Schönhense *et al.*, Nat. Commun. **5**, 3974 (2014).

[21] Z. Wen, H. Sukegawa, S. Kasai, K. Inomata, and S. Mitani, Phys. Rev. Appl. **2**, 024009 (2014).

[22] Z. Wen, H. Sukegawa, T. Furubayashi, J. Koo, K. Inomata, S. Mitani, J. P. Hadorn, T. Ohkubo, and K. Hono, Adv. Mater. **26**, 6483 (2014).

[23] Q. Qin, S. He, W. Song, P. Yang, Q. Wu, Y. P. Feng, and J. Chen, Appl. Phys. Lett. **110**, 112401 (2017).

[24] M. Belmeguenai, H. Tuzcuoglu, M. S. Gabor, T. Petrisor, Jr., C. Tiusan, D. Berling, F. Zighem, T. Chauveau, S. M. Chérif, and P. Moch, Phys. Rev. B **87**, 184431 (2013).

[25] S. Qiao, S. Nie, J. Zhao, Y. Huo, Y. Wu, and X. Zhang, Appl. Phys. Lett. **103**, 152402 (2013).

[26] S. Mizukami, D. Watanabe, M. Oogane, Y. Ando, Y. Miura, M. Shirai, and T. Miyazaki, J. Appl. Phys. **105**, 07D306 (2009).

[27] S. Husain, S. Akansel, A. Kumar, P. Svedlindh, and S. Chaudhary, Sci. Rep. **6**, 28692 (2016).

[28] A. Köhler, L. Wollmann, D. Ebke, S. Chadov, C. Kaiser, Z. Diao, Y. Zheng, Q. Leng, and C. Felser, Phys. Rev. B **93**, 094410 (2016).

[29] Y. Kasatani, S. Yamada, H. Itoh, M. Miyao, K. Hamaya, and Y. Nozaki, Appl. Phys. Express **7**, 123001 (2014).

[30] L. Hongzhi, Z. Zhiyong, M. Li, X. Shifeng, L. Heyan, Q. Jingping, L. Yangxian, and W. Guangheng, J. Phys. D **40**, 7121 (2007).

[31] Y.-P. Wang, J.-J. Qiu, H. Lu, R. Ji, G.-C. Han, and K.-L. Teo, J. Phys. D **47**, 495002 (2014).

[32] H. X. Yang, M. Chshiev, B. Dieny, J. H. Lee, A. Manchon, and K. H. Shin, Phys. Rev. B **84**, 054401 (2011).

[33] J. Koo, S. Mitani, T. Sasaki, H. Sukegawa, Z. Wen, T. Ohkubo, T. Niizeki, K. Inomata, and K. Hono, Appl. Phys. Lett. **103**, 192401 (2013).

[34] See Supplemental Material at http://link.aps.org/supplemental/10.1103/PhysRevMaterials.1.064401 for detailed structural analysis, magnetic properties, experimental and calculation methods.

[35] P. Webster, J. Phys. Chem. Solids **32**, 1221 (1971).

[36] Y. Miura, K. Nagao, and M. Shirai, Phys. Rev. B **69**, 144413 (2004).

[37] A. Sakuma, J. Phys. D **48**, 164011 (2015).

[38] Y.-P. Wang, G.-C. Han, H. Lu, J. Qiu, Q.-J. Yap, and K.-L. Teo, J. Appl. Phys. **115**, 17C301 (2014).

[39] T. L. Gilbert, Phys. Rev. **100**, 1243 (1955).

[40] O. Hjortstam, K. Baberschke, J. M. Wills, B. Johansson, and O. Eriksson, Phys. Rev. B **55**, 15026 (1997).

[41] B. Heinrich, C. Burrowes, E. Montoya, B. Kardasz, E. Girt, Y.-Y. Song, Y. Sun, and M. Wu, Phys. Rev. Lett. **107**, 066604 (2011).

[42] H. Chang, P. Li, W. Zhang, T. Liu, A. Hoffmann, L. Deng, and M. Wu, IEEE Magn. Lett. **5**, 1 (2014).

[43] V. Kamberský, Can. J. Phys. **48**, 2906 (1970).

[44] Y. Du, G. Xu, E. Liu, G. Li, H. Zhang, S. Yu, W. Wang, and G. Wu, J. Magn. Magn. Mater. **335**, 101 (2013).

[45] J. Lindner, I. Barsukov, C. Raeder, C. Hassel, O. Posth, R. Meckenstock, P. Landeros, and D. L. Mills, Phys. Rev. B **80**, 224421 (2009).

[46] J. Smit and H. G. Beljers, Philips Res. Rep. **10**, 113 (1955).

[47] M. Farle, Rep. Prog. Phys. **61**, 755 (1998).

[48] C. Vittoria, R. Barker, and A. Yelon, Phys. Rev. Lett. **19**, 792 (1967).

[49] J. Seib, D. Steiauf, and M. Fahnle, Phys. Rev. B **79**, 092418 (2009). .

[50] K. Gilmore, M. D. Stiles, J. Seib, D. Steiauf, and M. Fahnle, Phys. Rev. B **81**, 174414 (2010).

[51] H. Suhl, Phys. Rev. **97**, 555 (1955).

[52] A. Okada, S. Kanai, M. Yamanouchi, S. Ikeda, F. Matsukura, and H. Ohno, Appl. Phys. Lett. **105**, 052415 (2014).

[53] W. Platow, A. N. Anisimov, G. L. Dunifer, M. Farle, and K. Baberschke, Phys. Rev. B **58**, 5611 (1998).

[54] R. Arias and D. L. Mills, Phys. Rev. B **60**, 7395 (1999).

[55] M. Hurben and C. Patton, J. Appl. Phys. **83**, 4344 (1998).

[56] M. Körner, K. Lenz, R. A. Gallardo, M. Fritzsche, A. Mücklich, S. Facsko, J. Lindner, P. Landeros, and J. Fassbender, Phys. Rev. B **88**, 054405 (2013).

[57] G. Woltersdorf and B. Heinrich, Phys. Rev. B **69**, 184417 (2004).

[58] S. S. Kalarickal, P. Krivosik, J. Das, K. S. Kim, and C. E. Patton, Phys. Rev. B **77**, 054427 (2008).

[59] P. Krivosik, N. Mo, S. Kalarickal, and C. E. Patton, J. Appl. Phys. **101**, 083901 (2007).